Title

Tau PET and multimodal brain imaging in patients at risk for chronic traumatic encephalopathy.

Authors

Lesman-Segev, Orit H
La Joie, Renaud
Stephens, Melanie L
et al.

Publication Date

2019

DOI

10.1016/j.nicl.2019.102025

Peer reviewed

NeuroImage: Clinical 24 (2019) 102025

Contents lists available at ScienceDirect

NeuroImage: Clinical

journal homepage: www.elsevier.com/locate/ynicl

Tau PET and multimodal brain imaging in patients at risk for chronic traumatic encephalopathy

Orit H Lesman-Segev[a,*], Renaud La Joie[a], Melanie L Stephens[a], Ida Sonni[c], Richard Tsai[a], Viktoriya Bourakova[a], Adrienne V Visani[a], Lauren Edwards[a], James P O'Neil[c], Suzanne L Baker[c], Raquel C Gardner (MD)[a,d], Mustafa Janabi[c], Kiran Chaudhary[a], David C Perry[a], Joel H Kramer[a], Bruce L Miller[a], William J Jagust[c,e], Gil D Rabinovici[a,b,c,e]

[a] Memory and Aging Center, Department of Neurology, Weill Institute for Neurosciences, University of California, San Francisco, CA, 94158, United States
[b] Departments of Radiology and Biomedical Imaging, University of California San Francisco, San Francisco, CA 94158, United States
[c] Life Sciences Division, Lawrence Berkeley National Laboratory, Berkeley, CA 94720, United States
[d] San Francisco Veterans Affairs Medical Center, San Francisco, CA 94121, United States
[e] Helen Wills Neuroscience Institute, University of California Berkeley, Berkeley, CA 94720, United States

ARTICLE INFO

Keywords:
Chronic traumatic encephalopathy (CTE)
Imaging
Positron emission tomography (PET)
Tau
Amyloid
Magnetic resonance imaging (MRI)

ABSTRACT

Objective: To characterize individual and group-level neuroimaging findings in patients at risk for Chronic Traumatic Encephalopathy (CTE).

Methods: Eleven male patients meeting criteria for Traumatic Encephalopathy Syndrome (TES, median age: 64) underwent neurologic evaluation, 3-Tesla MRI, and PET with [^{18}F]-Flortaucipir (FTP, tau-PET) and [^{11}C]-Pittsburgh compound B (PIB, amyloid-PET). Six patients underwent [^{18}F]-Fluorodeoxyglucose-PET (FDG, glucose metabolism). We assessed imaging findings at the individual patient level, and in group-level comparisons with modality-specific groups of cognitively normal older adults (CN). Tau-PET findings in patients with TES were also compared to a matched group of patients with mild cognitive impairment or dementia due to Alzheimer's disease (AD).

Results: All patients with TES sustained repetitive head injury participating in impact sports, ten in American football. Three patients met criteria for dementia and eight had mild cognitive impairment. Two patients were amyloid-PET positive and harbored the most severe MRI atrophy, FDG hypometabolism, and FTP-tau PET binding. Among the nine amyloid-negative patients, tau-PET showed either mildly elevated frontotemporal binding, a "dot-like" pattern, or no elevated binding. Medial temporal FTP was mildly elevated in a subset of amyloid-negative patients, but values were considerably lower than in AD. Voxelwise analyses revealed a convergence of imaging abnormalities (higher FTP binding, lower FDG, lower gray matter volumes) in frontotemporal areas in TES compared to controls.

Conclusions: Mildly elevated tau-PET binding was observed in a subset of amyloid-negative patients at risk for CTE, in a distribution consistent with CTE pathology stages III-IV. FTP-PET may be useful as a biomarker of tau pathology in CTE but is unlikely to be sensitive to early disease stages.

1. Introduction

Chronic Traumatic Encephalopathy (CTE) is a neurodegenerative tauopathy associated with repetitive head impacts (RHI) (Mez et al., 2017; McKee et al., 2013). The post-mortem diagnosis of CTE is based on the identification of aggregated hyper-phosphorylated tau (p-tau) in neurons and astrocytes in a characteristic distribution in perivascular spaces and in the depth of cortical sulci (Mez et al., 2017; McKee et al., 2013; Baugh et al., 2014). Co-pathologies, including aggregated amyloid-beta (Aβ), alpha-synuclein, and transactive response DNA binding protein 43 kilodalton inclusions, are often found in advanced disease stages. Non-specific macroscopic features include gray matter atrophy, ventricular enlargement and septal abnormalities (McKee et al., 2013).

Traumatic Encephalopathy Syndrome (TES) defines a clinical syndrome associated with RHI (Reams et al., 2016; Montenigro et al., 2014; Jordan, 2013; Victoroff, 2013). Clinical features include

* Corresponding author.
E-mail address: lesmano@gmail.com (O.H. Lesman-Segev).

https://doi.org/10.1016/j.nicl.2019.102025
Received 6 May 2019; Received in revised form 3 September 2019; Accepted 27 September 2019
Available online 17 October 2019

behavioral, mood, cognitive and motor changes (Mez et al., 2017; McKee et al., 2013; Baugh et al., 2014; Gardner et al., 2015) that often present years after exposure to head trauma. Provisional research diagnostic criteria for TES have been proposed by several groups, however, there are no consensus criteria to date, and efforts are ongoing to validate clinical features that best predict underlying CTE neuropathology (Mez et al., 2015; Diagnose-CTE Research).

The diagnosis of CTE can be only made postmortem. Diagnosing CTE during life is challenging due to the clinical diversity of TES, the lack of verified consensus criteria and the lack of validated in-vivo biomarkers (Gardner et al., 2015). Adding neuroimaging biomarkers that identify the disease's core pathologic features may improve in-vivo diagnostic abilities. MRI and fludeoxyglucose positron emission tomography (FDG-PET) can detect structural and functional neurodegenerative changes respectively, while radiotracers specific for tau and Aβ could be helpful in detecting the molecular pathology of CTE and excluding underlying Alzheimer's disease (AD). Previous studies utilizing structural MRI found higher rates and larger size of cavum septum pellucidum (CSP) as well as more pronounced atrophy in patients at risk for CTE compared with aged matched controls (Little et al., 2014; Orrison et al., 2009; Gardner et al., 2016; Koerte et al., 2015). In addition, hypometabolism on FDG-PET was reported in at-risk patients (Gardner et al., 2015; Bang et al., 2015; Provenzano et al., 2010; Peskind et al., 2011). A recent study comparing Aβ (^{18}F-florbetapir) and tau (^{18}F-flortaucipir, FTP) PET findings in 26 symptomatic retired professional American football players versus 31 matched controls found higher FTP retention in bilateral frontotemporal and left parietal lobes in patients at risk for CTE (Stern et al., 2019). Amyloid positivity was not significantly different between the groups. Other studies utilizing Aβ and tau-PET are limited to case reports and small case series (Mitsis et al., 2014; Dickstein et al., 2016; Barrio et al., 2015; Omalu et al., 2017).

The goal of this study was to characterize multi-modal brain imaging findings in patients meeting TES criteria who are at risk for CTE. Findings were compared to cognitively normal controls without known exposure to RHI, and tau-PET findings were compared to patients with AD. We hypothesized that MRI and FDG-PET would identify neurodegenerative changes in the frontotemporal cortex, while tau-PET signal would be elevated in similar regions in patients with and without elevated Aβ-PET signal.

2. Methods

2.1. Patients with TES

We recruited consecutive patients exposed to RHI (Table 1) who presented with neurologic complaints at the University of California San Francisco (UCSF) Memory and Aging Center between August 2014 and October 2017. Patients were required to meet criteria for TES as proposed by Montenigro et-al[5]: history of multiple head impacts, no other neurological disorder that likely accounts for all clinical features, clinical symptoms present for more than 12 months, at least one core symptom including cognitive, mood or behavior, and two supportive features. To avoid circularity, we did not include tau-PET results as one of the factors considered for TES diagnosis. As part of the research evaluation, all participants underwent a detailed history and physical examination by a neurologist, a structured caregiver interview by a nurse, a battery of neuropsychological tests (Ossenkoppele et al., 2016), and multimodal brain imaging, including structural 3T MRI, ^{11}C-Pittsburgh compound B (PIB) Aβ-PET and ^{18}F-Flortaucipir (FTP) tau-PET. A subset of patients also underwent ^{18}F-FDG-PET. The average intervals between PET and MRI, PET and clinical testing, and MRI and clinical testing were 20 days (range: 1–69), 21 days (range: 1–68), and 6 days (range: 0–63), respectively.

2.2. Control groups

Imaging findings in patients with TES were compared to findings in cognitively normal controls (CN). FTP-PET in patients with TES was additionally compared to FTP in patients with AD. CN without known history of RHI were recruited from an aging cohort at UCSF (Staffaroni et al., 2018) for MRI and FDG, and from the Berkeley Aging Cohort Study (BACS) for all PET modalities (Maass et al., 2017). In order to optimally match for scanner, demographics and clinical characteristics, we compared each imaging modality in the TES group to a distinct control group (Table 2):

2.2.1. FTP-PET control groups

The FTP-PET healthy control group consisted of 67 Aβ-PET negative individuals. Due to limited availability of male only FTP data, both males and females were included. FTP controls were matched to the TES patients for education and age range. However, due to limitations of available data, the FTP controls were older than the TES group (median age at PET: 76 in the CN group versus 64 in the TES group).

The FTP-PET disease control group consisted of 22 males and females (due to limited availability of male only FTP data) patients from UCSF research cohorts meeting clinical criteria for mild cognitive impairment (MCI) or dementia due to AD (McKhann et al., 2011) with positive Aβ-PET and no known history of RHI. AD patients were matched on age and education to the TES patients (Mann-Whitney U-tests, $p > 0.56$). Patients with probable AD were classified as MCI or dementia stage based on the Clinical Dementia Rating (CDR) (Morris, 1993).

2.2.2. The FDG-PET control group consisted of 30 aβ-negative males matched on age and education to the TES group (Mann-Whitney U-tests, $p > 0.08$).

##

2.2.3. MRI control groups

The healthy control group for group voxel-wise analysis consisted of 54 males matched on age and education to the TES group (Mann-Whitney U-tests, $p > 0.08$) and scanned on the same two MRI scanners as the TES patients. Amyloid status was not available for this group.

For individual atrophy level assessment, w-maps (see below) were computed from a healthy control group dataset published by Potvin et al. (2017).

2.3. Patients and study participants

Written informed consent was obtained from all participants or their surrogate decision makers. The UCSF, University of California Berkeley and Lawrence Berkeley National Laboratory (LBNL) institutional review boards for human research approved the study.

2.4. Assessment of neuropsychological test scores

The neuropsychological battery included: the California verbal learning test (second edition) (Delis, 2000) and a test of recall of the Benson figure (Kramer et al., 2003) to assess episodic memory; forward and backward digit span (Rabinovici et al., 2015), Stroop color naming and inhibition (Stroop, 1935), modified Trail-making (Kramer et al., 2003), design fluency (Homack et al., 2005), phonemic fluency (words beginning with the letter 'D'/minute) (Kramer et al., 2003), and semantic fluency (animals/minute) (Kramer et al., 2003) to assess executive functioning; the 15-item Boston Naming Test (Homack et al., 2005) to assess language; the Benson figure copy to asses visuospatial skills; and the Geriatric Depression Scale (GDS) (Yesavage et al., 1982).

Neuropsychological test scores were standardized (z-transformed) based on age- and education-matched healthy control performance. We used a cutoff score of $-1.5 \leq z \leq -1.1$ to designate mild clinical impairment and $Z \leq -1.5$ to designate moderate to severe clinical

Table 1.
Patient characteristics.

	Sex	Race[1]	Age (decade[1])	Education	Impact sport exposure	Years in impact sport	Position played[1]	Main presenting symptoms	CDRtotal	CDR SB	MMSE	ApoE status[1]	[^{11}C]PIB status
Pt1	M		60s	18	NFL	13 (6 as pro.)		Memory, executive, visuospatial, language, behavior	1.0	7.0	4		Diffuse pos
Pt2	M		70s	16	NFL	20 (12 as pro.)		Memory, executive, visuospatial, behavior	1.0	4.5	24		Focal pos
Pt3	M		40s	16	College football, Other	11		Behavior, memory, language	0.5	4.0	22		Neg
Pt4	M		70s	16	NFL	21 (11 as pro.)		Memory, executive, headaches	0.5	1.0	27		Neg
Pt5	M		60s	16	NFL, Other	17 (9 as pro.)		Behavior, motor, memory, blackout episodes	0.5	3.5	28		Neg
Pt6	M		60s	16	Baseball, College football	8		Memory, executive, language, visuospatial, behavior	0.5	2.0	27		Neg
Pt7	M		40s	18	Rugby, HS football	9		Memory, post-traumatic epilepsy	0.5	0.5	29		Neg
Pt8	M		30s	16	NFL, wrestling	23 (3 as pro.)		Mood, sleep	0.5	2.5	27		Neg
Pt9	M		60s	16	NFL	18 (8 as pro)		Executive, minimal memory	0.5	2.0	27		Neg
Pt10	M		60s	14	Other	11		Memory, executive	0.5	3.5	25		Neg
Pt11	M		50s	16	NFL	18 (2 as pro.)		Executive, memory, visuospatial, mood	1.0	4.5	27		Neg
All TES Patients, *n* = 11	**100% M**	**82% - W 9% - B 9% - Mixed**	**60 s (30s-70 s)**	**16 (14–18)**	**7 retired NFL 4 other contact sports**	**–**	**Detailed description in the legend[2]**	**–**	**CDR 1: 3 CDR 0.5: 8**	**3 (0.5–7)**	**24 (4–29)**	**E3/3: 63.6% E2/4: 18.2% E3/4: 9.1% E2/2: 9.1%**	**2 Pos 9 Neg**

[1] - Specific ages, race, positions played and individual ApoE genotyping are not given to maintain anonymity.

[2] – Number of individuals in each position: defensive line: 2; linebacker: 3; defensive back: 2; special teams: 4; offensive lineman: 2; quarterback: 2; running back: 1; wide receiver: 1; no record: 1; no football exposure: 1; Some individuals played more than one position.

Abbreviations: AD – Alzheimer's disease; TES – Traumatic Encephalopathy Syndrome; CDR – Clinical Dementia Rating; SB – Sum of Boxes; Pt – Patient; Pro. - Professional; NFL – National Football League; Pos – Positive; Neg – Negative; HS – High school; FTP = flortaucipir; FDG – fludeoxyglucose; M – male; W – White, B – Black/African-American;

Continuous variables are presented as mean (range).

Table 2.
Control groups characteristics.

Control group	FTP PET HC	FDG PET HC	MRI HC	MRI HC by Potvin et-al*	AD disease control group
Used for	Tau PET w-maps, mean SUVR comparison, group voxel-wise *t*-test, and frequency maps analysis	Group voxel-wise *t*-test analysis	Group voxel-wise *t*-test analysis	Individual atrophy level assessment	Mean SUVR comparison, and frequency map analysis
Inclusion criteria	CDR 0, age range 20–95, negative Aβ-PET, no RHI	Males, CDR 0, age range 20–95 negative Aβ-PET, no RHI	Males, CDR 0, age range 20–95, no RHI	Adopted from Potvin et-al 2017, an open database of 2757 cognitively healthy males and females, aged 18–94, 82%- W, 10% B, 7% A*	Meet NIA-AA criteria for AD dementia or MCI, positive Aβ-PET, no RHI
Recruited from	Berkeley aging cohort study (BACS) - volunteer based healthy aging cohort	Aging cohort at UCSF and BACS	Aging cohort at UCSF		UCSF ADC cohorts
Number	67	30	54		22
Sex	55% males	100% males	100% males		23% males
Age (mean, range)	66 (20–93)	64 (26–80)	66 (33–86)		64 (48–82)
Education (mean, range)	17 (13–20)	17 (12–22)	17 (12–20)		17 (14–24)
Race	91% - W 6% - A 1.5% - M 1.5% - O	80% - W 3.3%-B 3.3% – M 13.3% - U	81.5% - W 1.8% - A 1.8% - O 14.8% - U		86.4 – W 4.5% - B 9.1% - U
MMSE (mean, range)	29 (25–30)	29 (27–30)	29 (26–30)		21 (8–28)
ApoE status	E3/3 74.5% E3/4 12.7% E2/3 12.7%	E3/3 70.4% E3/2 3.7% E3/4 25.9%	E3/3 57.4% E3/4 25.9% E2/2 1.8% E2/3 11.1% E4/4 3.7%		E3/3 28.6% E3/4 52.4% E4/4 14.3% E2/4 4.8%
Amyloid PET status	All negative	All negative	n/a	n/a	All positive

Abbreviations: HC – Healthy Controls; PET - Positron Emission Tomography; MRI - Magnetic Resonance imaging; MCI – Mild cognitive Impairment; SUVR - Standardized Uptake Value Ratio; NIA-AA - National Institute on Aging Alzheimer's Association; Aβ – Amyloid beta; BACS – Berkeley Aging Cohort; UCSF - University of California, San Francisco; MMSE - Mini-Mental State Examination; W - White; A - Asian; B – Black/African American; O - Other; U - Unreported; M - Mixed; ApoE - Apolipoprotein E; n/a - not applicable; AD – Alzheimer's disease; TES – Traumatic Encephalopathy Syndrome; CDR – Clinical Dementia Rating; FTP = flortaucipir; FDG – fludeoxyglucose.
* Potvin et-al, NeuroImage, 2017, doi:10.1016/j.neuroimage.2017.05.019.

impairment.

2.5. Neuroimaging acquisition

2.5.1. MRI

Structural T1-weighted MRI was acquired using magnetization prepared rapid acquisition gradient echo (MPRAGE) sequence on a 3T Siemens Tim Trio scanner ($N = 5$) or 3T Siemens MAGNETOM Prisma (Siemens Medical Systems) ($N = 6$) at the UCSF neuroimaging center as previously described (Ossenkoppele et al., 2016). Both scanners had very similar acquisition parameters (sagittal slice orientation; slice thickness = 1.0 mm; slices per slab = 160; in-plane resolution = 1.0 × 1.0 mm; matrix = 240×256; repetition time = 2,300 ms; inversion time = 900 ms; flip angle = 9°), although echo time differed slightly (Trio: 2.98 ms; Prisma: 2.90 ms).

2.5.2. PET

PIB-, FTP-, and FDG-PET scans were performed at LBNL on a Siemens Biograph 6 Truepoint PET/CT scanner in 3D acquisition mode. All PET scans were acquired within a short time period. PIB and FTP were typically acquired sequentially on the same day, and FDG was acquired at least 24 h following previous PET. Range between first and last PET scans was 0 (if only PIB and FTP were acquired and both on the same day) to 47 days. A low-dose CT scan was performed for attenuation correction prior to all scans. PIB and FTP were synthesized at the LBNL Biomedical Isotope Facility. FDG was purchased from a commercial vendor (IBA Molecular). Injected doses were approximately 10 mCi for FTP, 15 mCi for PIB, and 5–10mCi for FDG. PET images were acquired and reconstructed as previously described (Ossenkoppele et al., 2016; Lehmann et al., 2013). We analyzed data acquired from 50–70 min post-injection (PIB), 80–100 min post injection (FTP), and 30–60 min post-injection (FDG).

2.6. Neuroimaging preprocessing

MPRAGE images were segmented and parcellated using FreeSurfer 5.3 (surfer.nmr.mgh.harvard.edu). For cerebellar gray parcellation we used the Spatially Unbiased Infratentorial (SUIT) atlas as previously described (Maass et al., 2017; Desikan et al., 2006; Diedrichsen et al., 2009).

PET frames were realigned, averaged and co-registered onto the corresponding MRI. We calculated standardized uptake value ratio (SUVR) images by dividing raw count maps by mean tracer binding in specific reference regions (pons for FDG, inferior cerebellar gray matter (GM) for FTP, and cerebellar GM for PIB) defined on the MRI, as previously described (Maass et al., 2017; Ossenkoppele et al., 2016; La Joie et al., 2017).

MRI was segmented into GM, white matter and cerebrospinal fluid using Statistical Parametric Mapping 12 (SPM12; Welcome Department of Imaging Neuroscience, Institute of Neurology, London, UK) and warped onto Montreal Neurological Institute (MNI) template space. We then used the corresponding patient-specific deformation matrices to warp the corresponding PET images to template space. Total Intracranial Volume (TIV) (Malone et al., 2015) was derived from SPM12 to be used in statistical analyses (see below).

2.7. Image analysis and assessments

All images were assessed qualitatively at the individual level by visual inspection of each image by two visual raters (OHLS and GDR)

who were not blinded to clinical data. Group level comparisons with CN (all imaging modalities) and AD (FTP only) were conducted using voxelwise and region of interest (ROI) analyses.

2.7.1. Assessment of amyloid positivity

Individual native space PIB-SUVR images were rated as positive or negative for cortical uptake by one of the visual raters (OHLS or GDR) (Rabinovici et al., 2011). Global SUVR values were also converted to centiloid values (see supplementary information for detailed description of the conversion and validation methods).

2.7.2. Assessment of FTP PET binding

2.7.2.1. Whole cortical and medial temporal lobe (MTL) mean SUVR. Native space cortical and MTL mean SUVR were calculated for all participants. Subject-specific cortical masks were prepared by combining all relevant parcellated Freesurfer ROIs. Global mean cortical SUVR was calculated as a weighted average across all cortical ROIs. Since uptake in TES patients was dominant in the medial aspects of the temporal lobe and since the MTL is known to accumulate tau pathology in CTE, we also calculated a weighted mean SUVR of the MTL, including bilateral FreeSurfer-defined entorhinal and parahippocampal cortices and amygdala. Hippocampus was not included in the ROI to avoid spill over from nonspecific binding in the adjacent choroid plexus.

2.7.2.2. Voxel-wise analysis of FTP binding. Group level analysis of FTP binding was performed using FTP-PET SUVR images warped to MNI space, masked by an average brain mask, and smoothed using a 4 mm isotropic Gaussian kernel. TES patients were compared to CN ($n = 67$, Table 2) using a two-sample *t*-test voxelwise analysis, including age as a covariate.

2.7.2.3. FTP w-score maps. To compute individual maps of abnormal FTP binding while accounting for age-related non-specific changes in brain FTP binding (Lowe et al.), voxelwise w-score (age-adjusted Z-score) maps were computed for every patient based on the FTP control group ($n = 67$, Table 2 (La Joie et al., 2012)). The concept and method of w-score calculation has been described in detail elsewhere (La Joie et al., 2018). In brief, we first ran a voxelwise regression model within the control group to estimate the effect of age on FTP binding. Based on this regression, FTP binding in each voxel in each patient can be attributed a w-score based on the normal control distribution. Control participant w-maps were computed similarly but with a "leave one out" method, meaning that each control was compared to the regression model based on the other 66 controls. The resulting w-score map was then thresholded at 1.645 (to represent the 95th percentile of a normal distribution) and binarized, resulting in a subject-specific map of abnormal voxels. The percentage of suprathreshold voxels in each patient's segmented gray and white matter image was calculated. We then computed group frequency maps by summing all thresholded and binarized w-maps for every group (all TES, PIB-negative TES, CN, MCI-AD and dementia-AD) and dividing the summed image by the number of subjects in each group. Thus, the value in each voxel in the frequency map represents the percentage of subjects in the group that have abnormal binding (based on a threshold of w-score > 1.645) in that location.

To summarize, FTP-PET outcome measures are presented at the individual and group levels. At the individual level, raw FTP SUVR maps, voxel-based w-maps, percentage of abnormal voxels (w-score > 1.645) and mean cortical and MTL SUVR are presented. At the group level, frequency maps and voxelwise analysis of the TES group as a whole, as well as the amyloid-negative subgroup, are presented in contrast with CN and patients with AD.

2.7.3. Assessment of MRI abnormalities

2.7.3.1. GM loss. Quantitative measures of regional cortical thickness, volumes of subcortical structures, and ventricular volumes were calculated against a normative data set described by Potvin et-al (Potvin et al., 2017). This normative dataset includes 2757 cognitively healthy males and females, aged 18–94 from 23 samples, provided by 21 independent research groups. Based on this dataset, predicted values of thickness/volume as well as z-scores were calculated for each TES patient assessing deviation from normality while accounting for age, sex, estimated TIV, scanner manufacture and magnetic field strength (Potvin et al., 2017).

2.7.3.2. CSP size. CSP length and width were measured for every patient by a radiologist (OHLS) that assessed the T1 images for a CSF-filled cavity between the leaflets of the septum pellucidum and then used the ITK-SNAP 2.4.0 annotation tool to measure CSP width (in coronal sections) and length (in axial sections).

2.7.3.3. Voxelwise analyses. Voxelwise contrasts between TES and CN ($n = 54$, Table 2) were performed in SPM12. Modulated, GM segmented images were warped to MNI space and smoothed to PET resolution (by 7.6 FWHM isotropic Gaussian kernel). A two-sample *t*-test model of SPM12 was implemented with age, scanner and estimated TIV as covariates.

2.7.4. Assessment of metabolism patterns

Voxelwise group-level contrasts of FDG in TES vs CN ($n = 30$, Table 2) were performed using the FDG-PET SUVR images warped to MNI space and smoothed by a 4 mm FWHM isotropic Gaussian kernel (SPM12). Comparisons were made using a two-sample *t*-test, adding age as a covariate.

2.8. Statistical analysis

Differences in demographic characteristics (age, education, MMSE) between TES patients and CN or AD patients were assessed using the Mann-Whitney U-test. For each voxelwise analysis (in all modalities mentioned above), pairwise contrasts were performed and resulting T maps were thresholded (based on uncorrected $p < 0.005$ at the voxel level with family wise error-corrected (fwe) $p < 0.05$ at the cluster level) and converted to effect size Cohen's d maps using the CAT12 toolbox (www.neuro.uni-jena.de/cat/). Maps were rendered on a 3D brain surface using BrainNet Viewer (Xia et al., 2013) (www.nitrc.org/projects/bnv/) using default interpolation.

3. Results

3.1. Patient's characteristics

Patient characteristics are summarized in Table 1. All eleven patients were exposed to RHI in sports; ten played American football, including seven at the professional level in the U.S. National Football League. All patients reported innumerable head impacts with between none to multiple (40–50) concussions (defined as head impact followed by loss of consciousness or amnesia/neurologic symptom). Since self-report estimates of concussions and sub-concussive blows are unreliable (Register-Mihalik et al., 2013), we report cumulative years of sports participation as a proxy (McKee et al., 2013; Mckee et al., 2018). Neuropsychiatric complaints varied across patients, with memory loss being the most common. Eight patients were diagnosed with mild cognitive impairment (based on CDR of 0.5) and 3 with mild dementia (CDR 1). Specific ages, race, ApoE genotypes, and positions played are not shown in order to maintain anonymity. On cognitive testing, patients with TES as a group showed impaired list learning, moderate memory difficulties, slightly slowed performance on a set shifting task, and mild difficulty with confrontation naming. However, results were highly variable across participants and overall less profound than deficits seen in MCI or dementia due to AD (Table 3, individual values of

Table 3
Neurocognitive assessments.

		TES (n = 11)	MCI due to AD (n = 9)	Dementia due to AD (n = 13)	Controls normative data
	Age	59 ± 13.6	65.4 ± 10.7	62.5 ± 9.5	50-64[#]
Episodic memory					
CVLT	CVLT learning (sum of 4 trials)	20.6 ± 5.8**	19.3 ± 3*	16.6 ± 5.2**	23-29[$]
	Correct 30''	5.1 ± 2.6**	4.1 ± 2.1**	2.2 ± 2.0**	8.2 ± 1.4
	Correct 10'	4.1 ± 3.1**	2 ± 2.6**	1.4 ± 2**	7.8 ± 1.4
	Cued Correct	5.0 ± 2.8**	3.4 ± 2.9**	1.7 ± 1.8**	8.1 ± 1.2
Benson Figure recall	Benson Figure 10' recall	8.8 ± 2.8**	2.7 ± 3.0**	4.4 ± 3.6**	12.6 ± 2.3
Executive functioning					
	Digits Forward	6.1 ± 1.4*	5.9 ± 1.3	5.6 ± 1.4*	7.2 ± .9
	Digits Backward	4.1 ± 1.2	4.0 ± 1.4	3.3.0 ± 1.4**	5.4 ± .1.3
	Stroop Color Naming	66.5 ± 21.2**	49.6 ± 25.8**	44.1 ± 18.2**	90.3 ± 12.9
	Stroop Inhibition	40.1 ± 29.4*	23.8 ± 12.2**	17 ± 12.9**	52.6 ± 9.6
	Modified Trails Time	39.7 ± 17.2*	67.7 ± 37.4**	106 ± 27.9**	26.8 ± 10.7
	Design Fluency	8.8 ± 3.7	6.5 ± 4.4**	4.2 ± 1.8**	11.4 ± 2.8
	Lexical Fluency	12.3 ± 4.4	11.6 ± 3.4*	8.6 ± 5.3**	15 ± 3.9
	Semantic Fluency	17.5 ± 7.8*	13.8 ± 4.8**	10.6 ± 7.2**	22.7 ± 4.7
Language					
	Boston naming total correct	12.8 ± 1.4**	13.3 ± 1.5*	11.1 ± 3.4**	14.5 ± .9
Visuospatial skills					
	Benson Figure Copy	15.6 ± .9	11.4 ± 3.9**	11.8 ± 4.9**	15.5 ± 1.1
Mood					
	Geriatric Depression Scale	10.8 ± 7.2*	3.8 ± 2.8	8.7 ± 6	0-9 normal; 10-19 mild; 20-30 severe

Values in the table represent mean ± standard deviation; Z-scores were computed compared to normative data and are marked with asterisk: * = $-1.5 \leq$ z-score ≤ -1.1; ** = z-score ≤ -1.6

[#] Controls normative data presented in the table are for ages 50–64 and education ≤16 years, CVLT normative values are presented for the age range of 60–69.

[$] Range of normal values. No standard deviation available.

Abbreviations: AD – Alzheimer's disease; TES – Traumatic encephalopathy syndrome; CN – cognitively normal; CVLT - California verbal learning test

the TES cohort are presented in supplementary Table 1). The TES group endorsed more depressive symptoms than controls and patients with AD.

3.2. PIB-PET

Two of the patients with TES were PIB-positive on visual read and quantitatively using centiloid values (12.2 threshold for positivity (La Joie et al., 2019)). Patient 1 had diffuse cortical uptake and a centiloid value of 53 (Fig. 1A), while patient 2 had focal areas of cortical uptake in the left frontal lobe and left posterior cingulate and a centiloid value of 16. Analyses of other imaging modalities were performed first for the whole TES group (PIB-positive and PIB-negative), and again separately for the PIB-negative subgroup (excluding the two amyloid-positive patients) in order to avoid the potential confound of AD pathology on imaging findings.

3.3. FTP-PET

Fig. 1 shows FTP images of all patients with TES. Patient 1 (diffusely PIB positive) exhibited diffuse, intense, cortical FTP uptake, with relative sparing of sensorimotor and occipital cortex (Fig. 1B). Cortical FTP w-scores were very high, reaching a maximum of 24 standard deviations above age-matched controls, with 71% of gray and white matter voxels classified as abnormal (Fig. 1B). This patient's mean cortical and MTL SUVR values were higher than all other TES patients or CN and fell within the range of patients with AD (Fig. 1C and D). Patient 2 (focal PIB positive) had a similar pattern of diffuse cortical FTP uptake, though with much lower intensity. W-score map showed 32.5% abnormally high voxels, mainly in temporal and frontal regions. Mean cortical and MTL SUVR values were slightly above age-matched controls, and in the lower range of AD patients (Fig. 1C and D). Patient 3 demonstrated uptake predominantly in temporal and frontal cortices, with 28.7% of voxels classified as abnormal. This frontotemporal predominant binding pattern was also apparent in three other PIB negative patients (patients 4–6). Global mean cortical binding in these cases was within the CN range, and slightly higher in the MTL. Patient 7 showed a "dot-like" pattern with a non-specific distribution of small clusters with mildly elevated binding. 10.5% of voxels were classified as abnormal. The dot-like pattern was also apparent in Patient 8 and in various control subjects that did not report head injury exposure (Fig. 2). Patients 9–11 did not show any clear region of elevated binding, with only 0.1–1.9% of voxels classified as abnormal. Mean global cortical and MTL SUVRs were in the range of CN for patients demonstrating either non-specific "dot-like" binding or no elevated binding.

FTP frequency maps revealed that up to 60% (7/11) of TES patients demonstrated supra-threshold FTP binding, mainly in the bilateral frontotemporal cortex, with additional foci in the medial and lateral parietal lobes (Fig. 3A). Restricting the analysis to PIB-negative patients only, a similar but more restricted frontotemporal pattern persisted with reduction in parietal signal. In contrast, w-score frequency maps of CN showed small and irregularly distributed clusters of abnormal voxels reaching a maximum of only 12% (8/67) of the group in any voxel. Frequency maps of patients with MCI due to AD reveal a more diffuse pattern of abnormality with most (8–9/9) patients with MCI due to AD demonstrating elevated binding in the temporal and parietal lobes, with variable involvement of frontal cortex. Patients with dementia due to AD showed the most diffuse pattern of abnormal binding, with all (13/13) patients showing abnormal binding in temporal, parietal and frontal cortices, sparing only primary unimodal cortices.

On voxelwise contrast with CN, patients with TES showed elevated FTP binding predominantly in the left inferior-posterior temporal lobe with medium to strong effect size (Cohen's d up to 1.1). When restricting the analysis to the PIB-negative subgroup, a more constricted region of elevated binding was seen in the left inferior temporal lobe with additional region of increased binding in the inferior frontal lobes

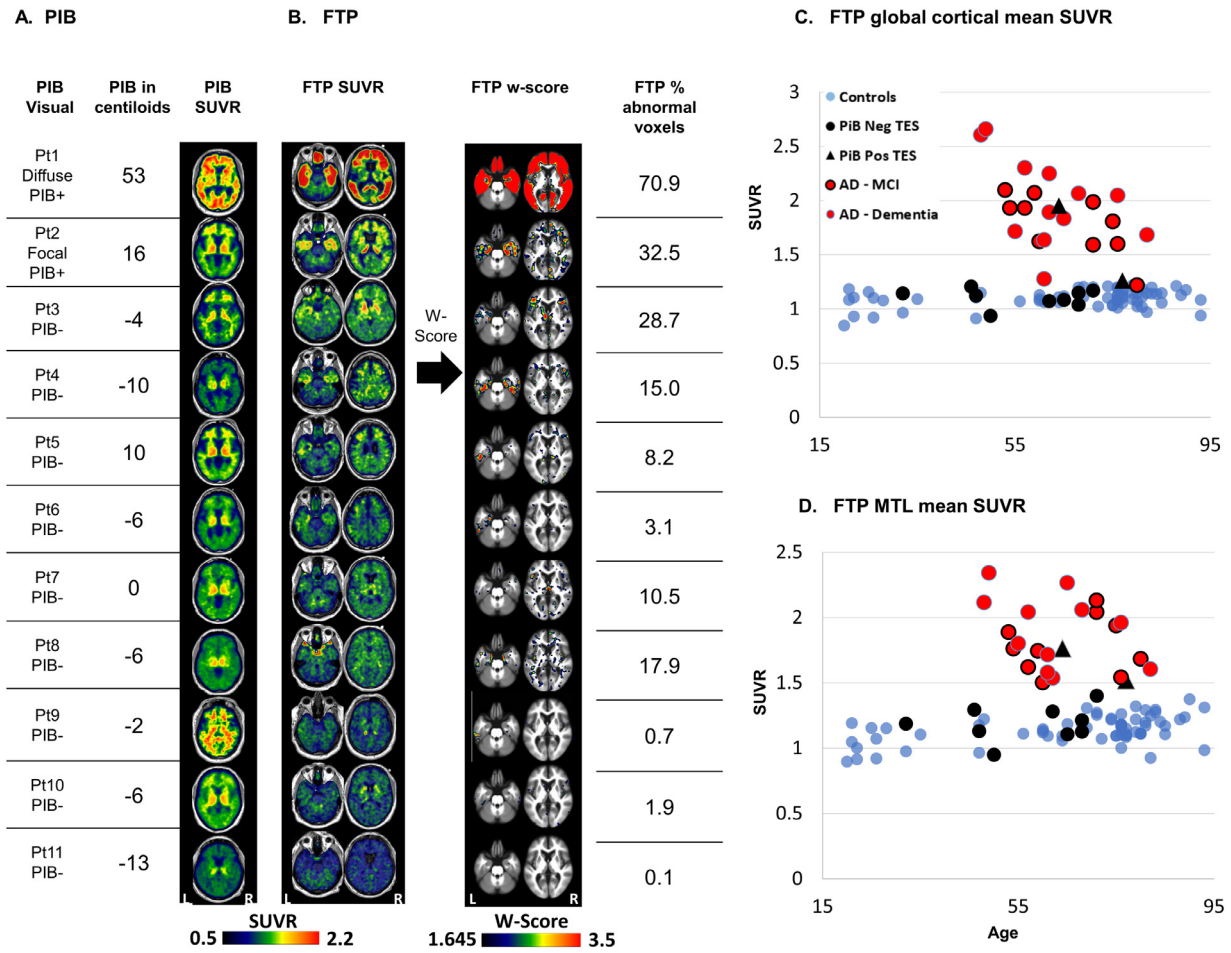

Fig. 1. Amyloid and tau PET patterns in TES, individual patterns.
Aβ (PIB)-PET visual read, centiloid value, and SUVR images (A); Tau (FTP)-PET SUVR images, w-score images, and percentage of voxels with w-score > 1.645 (B). Mean FTP-SUVR (C) and medial temporal lobe mean SUVR (D) in patients with TES (black triangles – PIB-positive; black circles – PIB-negative), patients with MCI (red circles black outline) or dementia due to AD (red circles no outline) and healthy controls (blue circles). The patient number on the left corresponds to the patient number in Table 1.
Images are presented in neurological convention (left of the image is the left side of the patient). Abbreviations- Pt = Patient; TES = traumatic encephalopathy syndrome; PIB = Pittsburgh compound B; PIB+ = positive visual read, PIB- = negative visual read; FTP = flortaucipir; MTL = medial temporal lobe; SUVR = standardized uptake value ratio; W-score = age adjusted z-score.(For interpretation of the references to colour in this figure legend, the reader is referred to the web version of this article.)

(Fig. 3B). No region of elevated binding was seen in TES patients compared with patients with MCI or dementia due to AD (supplementary figure 1), while many cortical regions showed higher binding in MCI/dementia due to AD compared with TES (supplementary figure and Fig. 3A).

3.4. Structural MRI

TES patients showed heterogeneous patterns of MRI GM loss (Fig. 4A and C). Some patients demonstrated cortical thinning (w-score < −1) compared to matched controls, some demonstrated mainly subcortical gray matter volume loss, and others did not show clear atrophy (w-score > −1). On average, the hippocampus showed the most severe volume loss (Fig. 4C). Eight of eleven patients had a CSP, with width ranging between 3 and 11 mm and length ranging between 1.5 and 45 mm (Fig. 4B). On voxelwise contrasts with CN, patients with TES showed lower GM volumes in the lateral and medial frontal cortices, insula and anterior temporal lobes (Cohen's d up to 1.5). This pattern was constrained to a smaller area when restricting the analysis to the PIB-negative subgroup (Fig. 4D).

3.5. FDG-PET

Six patients underwent FDG-PET in addition to amyloid- and tau-PET. Individual FDG SUVR images revealed primarily frontotemporal hypometabolism in addition to various degrees of parietal involvement. Patient 8 showed normal FDG uptake (Fig. 5A). As a group, patients with TES had significantly reduced metabolism mainly in the frontotemporal cortices with some parietal (precuneus and angular/supramarginal) involvement compared with CN (Cohen's d effect size up to 2.2). When restricting the analysis to the five PIB-negative patients that have FDG-PET (excluding patient 2), the frontotemporal cluster remained significant with large effect size (Cohen's d up to 2.1, Fig. 5B).

4. Discussion

In this study we applied multi-modal imaging to detect brain injury and molecular pathology in highly phenotyped patients meeting TES criteria who are at risk for CTE pathology. Tau-PET signal was highly elevated only in amyloid-positive patients, with more subtle uptake seen in a subset of amyloid-negative individuals, particularly in the frontal and temporal cortices. MRI and FDG changes were heterogeneous but tended to converge in frontotemporal regions. In summary,

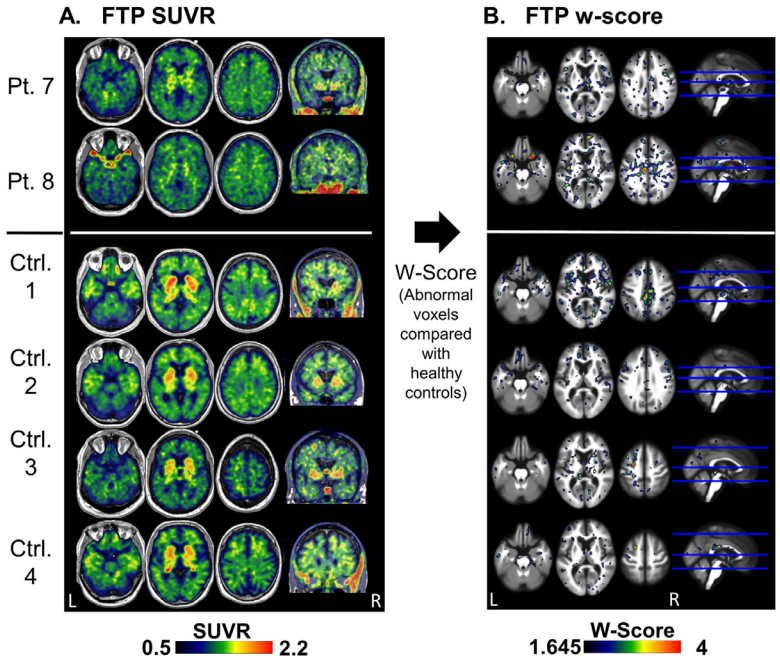

Fig. 2. Tau (FTP) PET "dot-like" pattern in TES patients and in CN
FTP SUVR (A) and w-score (B) images of two patients (patients 7 and 8) and four control subjects that have a non-specific distribution of small clusters with mildly elevated binding.
Abbreviations: FTP = flortaucipir; TES = traumatic encephalopathy syndrome; CN – cognitively normal control; Pt. – patient; Ctrl. – control; SUVR - standardized uptake value ratio; W-score = age adjusted z-score.

multi-modal imaging provides evidence for frontotemporal-predominant neurodegeneration and molecular pathology (tau more than amyloid) in individuals with TES, in line with the cognitive and behavioral deficits reported in this disorder.

Group-level elevated frontotemporal FTP binding was seen using both frequency maps and voxelwise analysis when comparing the entire TES cohort (n = 11) or the amyloid-negative subgroup (n = 9) to CN. An extensive and intense FTP binding pattern was observed in the amyloid-positive patients (patients 1 and 2), possibly due to primary AD pathology, with or without co-morbid CTE. The intensity of binding was lower in amyloid-negative patients with TES compared to patients with MCI or dementia due to AD. Four amyloid-negative patients with TES (patients 3–6) showed visually discernable and confluent regions of elevated FTP signal, predominantly in frontal and temporal cortices,

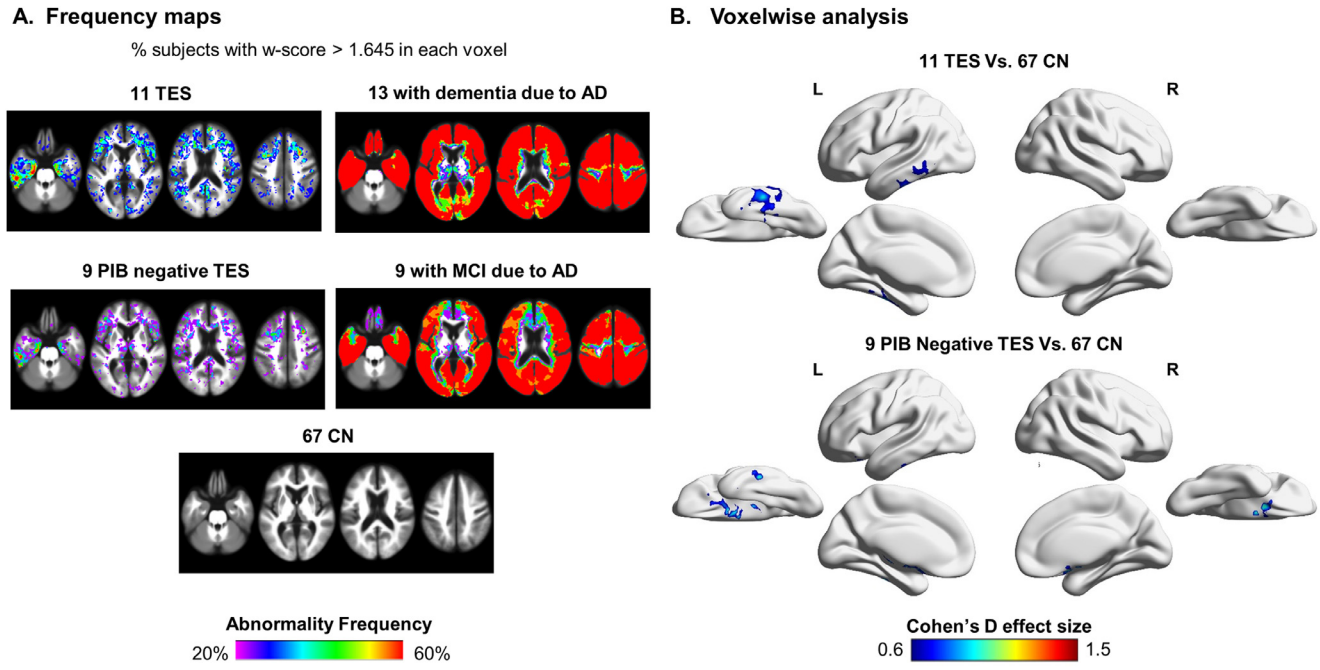

Fig. 3. Tau (FTP) PET in TES compared with CN and AD, group analysis
FTP binding frequency maps of the TES cohort (n = 11), the amyloid-negative subgroup of TES patients (n = 9), healthy controls (n = 67), patients with dementia due to AD (n = 13) and patients with MCI due to AD (n = 9). The value in each voxel represents the percentage of subjects that have high binding (defined here as w-score > 1.645) in that voxel (A). Voxelwise two sample t-test analysis reported in Cohen's d effect size of FTP-PET binding in the TES cohort (n = 11) and in the amyloid-negative subgroup of TES patients (n = 9) compared with 67 healthy controls, $P_{Uncorrected} < 0.005$ in the voxel level, $P_{fwe} < 0.05$ in the cluster level (B). Images are presented in neurologic convention. PIB = Pittsburg compound B; FTP = flortaucipir; Lat = lateral; Med = medial; Inf = inferior; TES – traumatic encephalopathy syndrome; AD = Alzheimer's disease; MCI = mild cognitive impairment; CN – cognitively normal control; CDR = clinical dementia score; FWE – family wise correction.

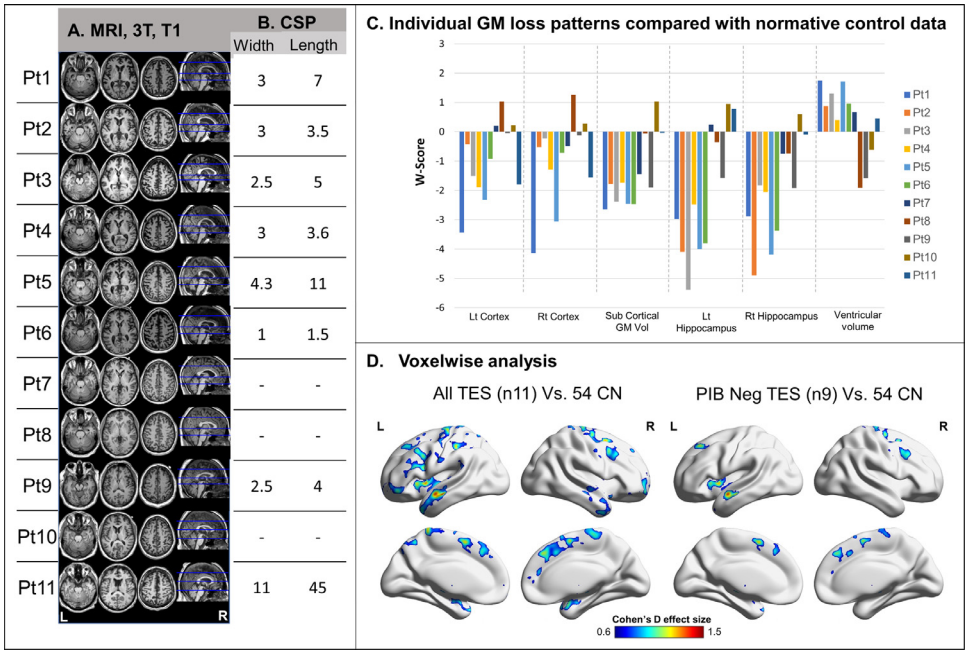

Fig. 4. Individual and group-level analysis of structural changes in TES patients
Axial T1 weighted MRI of all 11 patients with TES (A) including cavum Septum Pellucidum (CSP) width and length in millimeters (B). Individual atrophy patterns as represented by w-scores of bilateral cortical thickness, subcortical gray matter volume, bilateral hippocampal volume, and ventricular volume compared to normalized control data (based on Potvin et-al (Potvin et al., 2017)) (C). Group-level two sample *t*-test analysis of atrophy patterns ($P_{Uncorrected} < 0.005$ at the voxel level, $P_{fwe} < 0.05$ at the cluster level converted to Cohen's d effect size) in the whole TES cohort ($n = 11$) and the amyloid-negative subgroup only ($n = 9$) compared with 54 controls. Patient numbers correspond to the same numbers as in Table 1 and in the other figures.
TES – traumatic encephalopathy syndrome; CN – cognitively normal control; CSP – cavum septum pellucidum; GM – gray matter; Lt – left; Rt – right; Vol – volume; Pt – patient; FEW – family wise error corrected.

including the medial temporal lobe. In the absence of amyloid, this signal may be related to CTE tau pathology, with the distribution of binding consistent with CTE neuropathological stages III-IV (McKee et al., 2013). However, we cannot exclude the possibility that FTP is binding to an alternative form of tau (e.g. primary age-related tauopathy, or other non-AD tau isoforms (Smith et al., 2017; Schonhaut et al., 2017; Utianski et al., 2018)), or to non-tau related processes in these individuals, given some of the questions about tracer specificity (see limitations). Two amyloid-negative patients showed a "dot-like" pattern of binding, which could be consistent with the focal tau deposits seen in CTE stages I-II but was also seen in normal controls with no RHI. The remaining three patients showed no evidence of abnormal binding. These results may be due to an absence of CTE pathology in these individuals, or to lack of sensitivity of FTP-PET for detecting early stages of CTE.

All the amyloid-negative patients in our cohort demonstrated low FTP binding compared with patients with MCI or dementia due to AD. There are several potential interpretations of this finding. First, the low level of binding may be explained by a low burden of tau pathology. As our patient group is relatively small and consists of mostly young (median age of 64) and mildly impaired (CDR 0.5–1) patients, it is possible that some of them have early stage CTE bearing a low density of tau-positive aggregates. Others may have neuropathological processes other than tau underlying their symptoms. Additionally, it is possible that FTP may bind with weaker affinity to tau aggregates in CTE than in AD. Tau aggregates in CTE are similar, though not identical, to those seen in AD. Neuronal inclusions include paired helical filaments of hyper-phosphorylated tau composed of a mix of 3-repeat and 4-repeat tau isoforms, reflecting alternative splicing of the microtubule binding motif on exon 10, though the biochemical composition may be slightly skewed toward 4R isoforms in CTE compared to AD. CTE also features more axonal pathology and prominent astrocytic tau

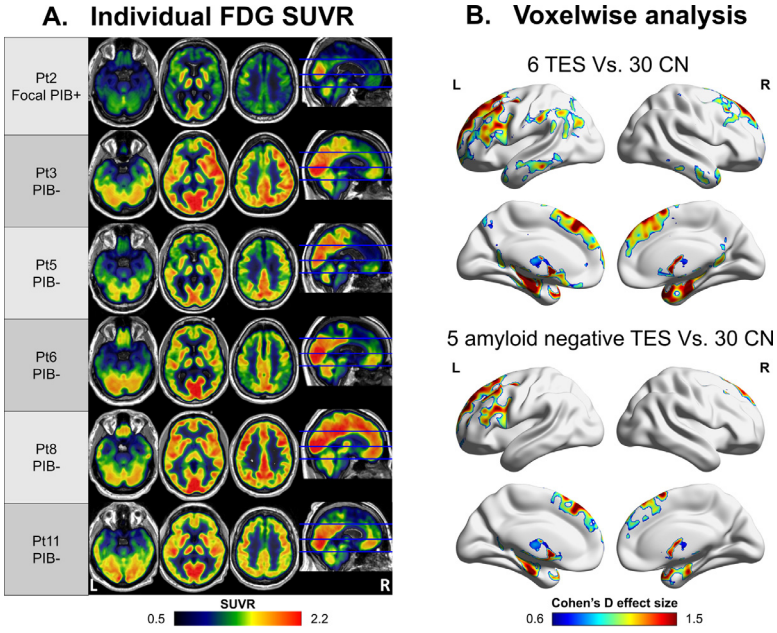

Fig. 5. Individual and group-level metabolism pattern
FDG-PET SUVR images of six patients with TES that underwent FDG-PET (A) and voxelwise two sample *t*-test analysis of the all patients and the five amyloid-negative patients compared with 30 controls. Reported in Cohen's d effect size, $P_{uncorrected} < 0.005$; cluster threshold: $P_{fwe} < 0.05$ (B). Patient numbers correspond to the same numbers as in Table 1 and in the other figures.
FDG – fluorodeoxyglucose; SUVR - standardized uptake value ratio; TES – traumatic encephalopathy syndrome; CN – cognitively normal control; FEW – family wise error correction.

inclusions, which are not a feature of AD (McKee et al., 2013). Moreover, it has been recently shown that the β-helix conformation of tau aggregates in CTE is distinct from other taupathies (Falcon et al., 2019). These differences in biochemical composition, post-translational modifications and microstructure could lead to a reduced detectability by routine tau CSF assays (Alosco et al., 2018) as well as reduced affinity of FTP to bind to tau aggregates in CTE. This possibility is supported by preliminary autoradiography data showing at least a 5-fold lower intensity of FTP binding in temporal cortex of stage III-IV CTE brain sections compared with AD brain sections (HAI-Book). Other studies have found lower FTP in vivo retention (Smith et al., 2017; Schonhaut et al., 2017; Utianski et al., 2018; Cho et al., 2017) and no or low autoradiography binding (Marquié et al., 2015; Sander et al., 2016; Lowe et al., 2016) in non-AD tauopathies, such as progressive supranuclear palsy, corticobasal degeneration and Pick's disease. Ultimately, correlational studies between FTP-PET and autopsy in the same individuals will be needed to narrow down these possibilities.

It has been recently shown that symptomatic former National Football League (NFL) players have higher FTP-PET binding in bilateral superior frontal, bilateral MTL and left parietal regions in the group level but individual binding levels overlap with binding in CN (Stern et al., 2019). Consistent with these findings, our group frequency maps demonstrate increased frontotemporal binding in a subset of at-risk patients. Previous case reports utilizing FTP imaging in patients at risk for CTE showed either striatal and nigral binding (Mitsis et al., 2014) or weak binding in the gray matter – white matter (GM-WM) interface (Dickstein et al., 2016). In our cohort, we also found striatal, nigral, and GM-WM matter interface FTP binding, but these were neither unique to nor more prominent in patients with TES compared with controls. Accordingly and based on other studies (Marquié et al., 2017), we interpret the striatal and nigral binding as “off-target” signal unrelated to tau. Also, though part of the signal we see in GM-WM interface may be detecting early CTE lesions, our data suggest that this signal is indistinguishable from noise. Other in-vivo studies using a different putative tau ligand, [^{18}F]FDDNP PET, demonstrated distinct binding patterns in patients at risk for CTE compared to controls (Barrio et al., 2015, Small et al., 2013). However, [^{18}F]FDDNP appears to be a non-selective tracer with affinity for β-pleated sheets composed of various aggregated proteins, including tau but also Aβ, prion protein, huntingtin and others (Smid et al., 2006). Additional limitations of [^{18}F]FDDNP include low signal-to-noise, and poor reproducibility of results across sites (Ossenkoppele et al., 2012).

Our results may indicate that early stages of CTE pathology are below the sensitivity of FTP-PET. Small numbers of low volume pathological foci are seen neuropathologically at early stages of CTE. These foci, estimated to be 1–5 mm in diameter in early disease stages (Mez et al., 2017; McKee et al., 2013), may be too small to detect given the limited spatial resolution of PET. In comparison, the resolution of our PET scanner (Siemens Biograph 6 Truepoint PET-CT scanner) is $6.5 \times 6.5 \times 7.25$ mm (calculated based on phantom (Joshi et al., 2009)). Moreover, due to the heterogeneity of head impacts, the location of tau varies across individuals at early disease stages. This heterogeneity becomes less pronounced in later stages as the disease progresses and the lesions become larger and more confluent, notably in the frontal and temporal cortices (McKee et al., 2013), likely facilitating their detection by molecular imaging.

Two patients in our series were PIB and tau PET positive (patients 1 and 2). This combination of amyloid and tau PET positivity may be attributed to primary AD pathology with or without co-morbid CTE, specifically for patient 1 that had extensive and intense binding of both amyloid and tau PET (La Joie et al., 2012). The focal amyloid positivity pattern together with the lower FTP binding seen in patient 2 may represent either early AD changes, CTE pathology with Aβ accumulation following trauma, or incidental/age-related amyloid positivity. Neuropathological studies have reported the presence of amyloid beta plaques both in the acute phase after a single severe traumatic brain injury (Roberts et al., 1991; Roberts et al., 1994; Ikonomovic et al., 2004) and in the chronic phase following RHI (Mez et al., 2017; McKee et al., 2013; Stein et al., 2015). In the acute phase, a rapid and usually focal accumulation of Aβ plaques was shown in up to 30% of patients, including children, who died acutely following severe TBI (Roberts et al., 1991; Roberts et al., 1994). In the chronic phase, recent series have reported that 52–61% (Stein et al., 2015; Mez et al., 2017) of patients with autopsy-proven CTE also have amyloid plaques (Mez et al., 2017; Stein et al., 2015). The plaques observed following TBI are similar but not identical to the ones deposited in AD. In AD, the plaques are more commonly neuritic, while post-TBI plaques are typically diffuse. The proportion of amyloid positivity in our series was smaller (2/11) compared to neuropathological reports (Stein et al., 2015; Mez et al., 2017). This discordance may be explained by small sample size, the relatively young age of our cohort, or possibly lower affinity of PIB for diffuse versus neuritic plaques (Seo et al., 2017; Ikonomovic et al., 2008).

We found variability in the presence and size of CSP and the degree of gray matter atrophy across patients. Our findings are in line with reported imaging findings in 100 boxers showing hippocampal atrophy in 59%, cerebral atrophy in 24%, ventricular size abnormalities in 19%, and CSP in 43% of patients (Orrison et al., 2009). Among the six patients who underwent FDG-PET, five showed hypometabolism in the temporal lobe and four had additional frontoparietal hypometabolism. These findings are consistent with a previous report from our group that demonstrated temporal hypometabolism in five retired National Football League players (Gardner et al., 2015) and other reports of similar patterns of hypometabolism in boxers (Provenzano et al., 2010) and war veterans with blast exposure (Peskind et al., 2011).

At the group level, we found a frontotemporal predominant abnormality pattern across neuroimaging modalities. Such an abnormality pattern is in line with the cognitive and behavioral predominant clinical presentation seen in our series and described in TES, suggesting an association between brain injury, tau binding, neurodegeneration (as expressed by atrophy and hypometabolism) and neuropsychiatric symptomatology. The extent and effect size, however, differ between modalities with FDG hypometabolism having the most widespread pattern and highest effect size (Cohen's d up to 2.2), followed by MRI atrophy measures, and then FTP binding (Cohen's $d < 1.5$ and 1.1 respectively). Atrophy and hypometabolism are considered to be downstream of tau deposition as well as other pathologies (i.e. axonal injury, cerebrovascular disease and other causes of white matter injury, or other proteinopathies). As such, MRI and FDG measures reflect the collective effects of all pathologies and may thus be more sensitive to trauma-related injury, though non-specific regarding the underlying mechanism of injury.

Strengths of this study include the application of multimodal neuroimaging utilizing both structural and molecular imaging in highly phenotyped patients meeting TES criteria, the comparison to a CN group as well as patients with AD (for FTP-PET), and the application of both individual and group-level analyses. Our study has limitations. The relatively small number of patients that reduces power for statistical analysis. It is possible that with more patients, larger variability in the amyloid negative tau-PET binding levels would have been seen, and together with higher statistical power uncover earlier stages of CTE pathology. Additional limitations include the lack of neuropathological validation, and the use of multiple control groups, some of which included both males and females while the TES group consists of males only. In a recent paper (Buckley et al., 2019) no clear association was found between sex and regional tau deposition in amyloid negative cognitively normal individuals. Thus, the inclusion of female controls is unlikely to have significantly impacted our results. Detailed athletic characteristics including age at first exposure were not assessed with a standard protocol in this retrospective study, and thus are not reported. Furthermore, due to varying acquisition protocols, we were not able to include diffusion tensor imaging (DTI), a sensitive imaging modality to

assess TBI-related white matter injury, in our MRI assessment. The specificity of FTP is challenged by binding in areas that are known to have minimal or no neurofibrillary tangles such as basal ganglia, choroid plexus, meninges, and cerebrovascular lesions (Lockhart et al., 2017; Bruinsma et al., 2017; Lee et al., 2018), as well as cortical binding in clinical syndromes, such as semantic variant primary progressive aphasia, that are usually caused by non-tau proteinopathies (Bevan-Jones et al., 2017; Makaretz et al., 2017). Nevertheless, we found FTP binding in frontotemporal regions in a distribution that is consistent with the neuropathology of CTE.

5. Conclusion

In this case series of eleven patients with TES at risk for CTE, we found a frontotemporal predominant pattern of brain injury at the group level across modalities. FTP binding in amyloid-negative patients was modest, predominantly affecting the temporal and frontal lobes in a subset of patients, potentially mirroring the distribution of pathology in CTE pathologic stages III-IV. FTP may detect tau pathology in CTE, though possibly in later stages of disease and with weaker binding compared with AD. Correlation with post-mortem findings and larger cohorts are needed to validate these findings.

Statistical analyseswere conducted by Orit Lesman-Segev, MD, Memory and Aging Center, University of California San Francisco, San Francisco, CA, United States

Disclosures of all authors' financial relationships:

- Dr. Orit H Lesman-Segev – none
- Dr. Renaud La Joie - none
- Dr. Melanie Stephens – none
- Dr. Ida Sonni - none
- Dr. Richard Tsai – is supported by grant K23AG055688 from the National Institute on Aging (NIA). He also consulted for ExpertConnect, Grifols and S.A.
- Ms. Viktoriya Bourakova - none
- Ms. Adrienne Visani - none
- Ms. Lauren Edwards - none
- Dr. James P O'Neil - none
- Dr. Suzanne L Baker - none
- Dr. Raquel C. Gardner - none
- Dr. Mustafa Janabi - none
- Ms. Kiran Chaudhary – none
- Dr. David Perry – is supported by grant K23AG045289 from the National Institute on Aging (NIA)
- Dr. Joel H Kramer – serves as a consultant for Biogen
- Dr. Bruce L Miller – receives grants in support of the Memory and Aging Center from the NIH/NIA, the Quest Diagnostics Dementia Pathway Collaboration, Cornell University and The Bluefield Project to Cure Frontotemporal Dementia. He serves as Medical Director for the John Douglas French Foundation; Scientific Director for the Tau Consortium; Director/Medical Advisory Board of the Larry L. Hillblom Foundation; and Past President of the International Society of Frontotemporal Dementia (ISFTD).
- Dr. William J Jagust - serves as a consultant to Bioclinica, Genentech, Novartis, and Biogen
- Dr. Gil D Rabinovici - receives research support from Avid Radiopharmaceuticals, Eli Lilly, GE Healthcare, and Life Molecular Imaging. He has received consulting fees from Axon Neurosciences, Eisai, Genentech, Merck and Roche and speaking honorarium from GE Healthcare. Associate Editor for JAMA Neurology.

Acknowledgments

Avid Radiopharmaceuticals enabled use of the [18F]Flortaucipir tracer by providing precursor, but did not provide direct funding and was not involved in data analysis or interpretation.

This work was supported by the National Institute on Aging grants (R01-AG045611; to G.D.R.), (R01-AG034570; to W.J.J.), (P50-AG023501; to B.L.M. and G.D.R); Tau Consortium(to G.D.R. and W.J.J) and the Alzheimer's Association (AARF-16-443577 to R.L.J).

The funding sources were not involved in the study design, collection, analyses, interpretation or writing.

Appendix 1. Authors

Name	Location	Role	Contribution
Orit H Lesman-Segev, MD	Memory and Aging Center, University of California San Francisco	Author	Design and conceptualized the study; analyzed the data; interpreted the data, drafted the manuscript for intellectual content
Renaud La Joie, PhD	Memory and Aging Center, University of California San Francisco	Author	Design the study; interpreted the data; revised the manuscript for intellectual content
Melanie Stephens, PhD	Memory and Aging Center, University of California San Francisco	Author	interpreted the data, revised the manuscript for intellectual content
Viktoriya Bourakova, BA	Memory and Aging Center, University of California San Francisco	Author	Major role in the acquisition of data, revised the manuscript for intellectual content
Adrienne Visani, BS	Memory and Aging Center, University of California San Francisco	Author	Major role in the acquisition of data, revised the manuscript for intellectual content
Lauren Edwards, BS	Memory and Aging Center, University of California San Francisco	Author	Major role in the acquisition of data, revised the manuscript for intellectual content
James P O'Neil, PhD	Life Sciences Division, Lawrence Berkeley National Laboratory	Author	Major role in the acquisition of data
Suzanne L Baker, PhD	Life Sciences Division, Lawrence Berkeley National Laboratory	Author	Major role in the acquisition of data; revised the manuscript for intellectual content
Raquel C. Gardner MD	Memory and Aging Center, University of California San Francisco; San Francisco Veterans Affairs Medical Center	Author	Major role in the acquisition of data; Revised the manuscript for intellectual content
Mustafa Janabi, PhD	Life Sciences Division, Lawrence Berkeley National Laboratory	Author	Major role in the acquisition of data; revised the manuscript for intellectual content
Kiran Chaudhary, MS	Memory and Aging Center, University of California San Francisco	Author	Major role in the acquisition of data; revised the manuscript for intellectual content
David Perry, MD	Memory and Aging Center, University of California San Francisco	Author	Major role in the acquisition of data; revised the manuscript for intellectual content
Joel H Kramer, PsyD	Memory and Aging Center, University of California San Francisco	Author	Major role in the acquisition of data; revised the manuscript for intellectual content
Bruce L Miller, MD	Memory and Aging Center, University of California San Francisco	Author	Major role in the acquisition of data; revised the manuscript for intellectual content
William J Jagust, MD	Life Sciences Division, Lawrence Berkeley National Laboratory	Author	Major role in the acquisition of data; revised the manuscript for intellectual content

Gil D Rabinovici, MD	Memory and Aging Center, Departments of Neurology, Radiology and Biomedical Imaging, University of California San Francisco; Life Sciences Division, Lawrence Berkeley National Laboratory; and Helen Wills Neuroscience Institute, University of California Berkeley	Author	Design and conceptualized study; interpreted the data; revised analysis; revised the manuscript for intellectual content

Supplementary materials

Supplementary material associated with this article can be found, in the online version, at doi:10.1016/j.nicl.2019.102025.

References

Alosco, M.L., Tripodis, Y., Fritts, N.G., et al., 2018. Cerebrospinal fluid tau, αβ, and sTREM2 in former national football league players: modeling the relationship between repetitive head impacts, microglial activation, and neurodegeneration. Alzheimers Dement. J. Alzheimers Assoc. 14 (9), 1159–1170. https://doi.org/10.1016/j.jalz.2018.05.004.

Bang, S.A., Song, Y.S., Moon, B.S., et al., 2015. Neuropsychological, metabolic, and GABAA receptor studies in subjects with repetitive traumatic brain injury. J. Neurotrauma 33 (11), 1005–1014. https://doi.org/10.1089/neu.2015.4051.

Barrio, J.R., Small, G.W., Wong, K.-P., et al., 2015. In vivo characterization of chronic traumatic encephalopathy using [F-18]FDDNP PET brain imaging. Proc. Natl. Acad. Sci. U. S. A. 112 (16), E2039–E2047. https://doi.org/10.1073/pnas.1409952112.

Baugh, C.M., Robbins, C.A., Stern, R.A., McKee, A.C, 2014. Current understanding of chronic traumatic encephalopathy. Curr. Treat. Options Neurol. 16 (9), 306. https://doi.org/10.1007/s11940-014-0306-5.

Bevan-Jones, W.R., Cope, T.E., Jones, P.S., et al., September 2017. [18F]AV-1451 binding in vivo mirrors the expected distribution of TDP-43 pathology in the semantic variant of primary progressive aphasia. J. Neurol. Neurosurg. Psychiatry. https://doi.org/10.1136/jnnp-2017-316402.

Bruinsma, T.J., Johnson, D.R., Fang, P., et al., 2017. Uptake of AV-1451 in meningiomas. Ann. Nucl. Med. 31 (10), 736–743. https://doi.org/10.1007/s12149-017-1205-0.

Buckley, R.F., Mormino, E.C., Rabin, J.S., et al., 2019. Sex differences in the association of global amyloid and regional tau deposition measured by positron emission tomography in clinically normal older adults. JAMA Neurol. 76 (5), 542–551. https://doi.org/10.1001/jamaneurol.2018.4693.

Cho, H., Baek, M.S., Choi, J.Y., et al., 2017. 18 F-AV-1451 binds to motor-related subcortical gray and white matter in corticobasal syndrome. Neurology 89 (11), 1170–1178. https://doi.org/10.1212/WNL.0000000000004364.

Delis, D, 2000. California Verbal Learning Test-Second Edition. Adult Version Man Psychol Corp.. https://ci.nii.ac.jp/naid/20001566093/ Accessed December 20, 2018.

Desikan, R.S., Ségonne, F., Fischl, B., et al., 2006. An automated labeling system for subdividing the human cerebral cortex on MRI scans into gyral based regions of interest. Neuroimage 31 (3), 968–980. https://doi.org/10.1016/j.neuroimage.2006.01.021.

Dickstein, D.L., Pullman, M.Y., Fernandez, C., et al., 2016. Cerebral [18 F]T807/AV1451 retention pattern in clinically probable CTE resembles pathognomonic distribution of CTE tauopathy. Transl. Psychiatry 6 (9), e900. https://doi.org/10.1038/tp.2016.175.

Diedrichsen, J., Balsters, J.H., Flavell, J., Cussans, E., Ramnani, N., 2009. A probabilistic MR atlas of the human cerebellum. Neuroimage 46 (1), 39–46. https://doi.org/10.1016/j.neuroimage.2009.01.045.

Falcon, B., Zivanov, J., Zhang, W., et al., March 2019. Novel tau filament fold in chronic traumatic encephalopathy encloses hydrophobic molecules. Nature 1. https://doi.org/10.1038/s41586-019-1026-5.

Gardner, R.C., Possin, K.L., Hess, C.P., et al., 2015. Evaluating and treating neurobehavioral symptoms in professional American football players. Neurol. Clin. Pract. 5 (4), 285–295. https://doi.org/10.1212/CPJ.0000000000000157.

Gardner, R.C., Hess, C.P., Brus-Ramer, M., et al., 2016. Cavum septum pellucidum in retired American pro-football players. J. Neurotrauma 33 (1), 157–161. https://doi.org/10.1089/neu.2014.3805.

HAI-Book-Jan-5.pdf. https://www.worldeventsforum.com/hai/wp-content/uploads/2016/12/HAI-Book-Jan-5.pdf. Accessed March 11, 2018.

Homack, S., Lee, D., Riccio, C.A, 2005. Test review: delis-Kaplan executive function system. J. Clin. Exp. Neuropsychol. 27 (5), 599–609. https://doi.org/10.1080/13803390490918444.

Ikonomovic, M.D., Uryu, K., Abrahamson, E.E., et al., 2004. Alzheimer's pathology in human temporal cortex surgically excised after severe brain injury. Exp. Neurol. 190 (1), 192–203. https://doi.org/10.1016/j.expneurol.2004.06.011.

Ikonomovic, M.D., Klunk, W.E., Abrahamson, E.E., et al., 2008. Post-mortem correlates of in vivo PiB-PET amyloid imaging in a typical case of alzheimer's disease. Brain J. Neurol. 131 (Pt 6), 1630–1645. https://doi.org/10.1093/brain/awn016.

Jordan, B.D., 2013. The clinical spectrum of sport-related traumatic brain injury. Nat. Rev. Neurol. 9 (4), 222–230. https://doi.org/10.1038/nrneurol.2013.33.

Joshi, A., Koeppe, R.A., Fessler, J.A, 2009. Reducing between scanner differences in multi-center PET studies. Neuroimage 46 (1), 154–159. https://doi.org/10.1016/j.neuroimage.2009.01.057.

Koerte, I.K., Hufschmidt, J., Muehlmann, M., et al., 2015. Cavum septi pellucidi in symptomatic former professional football players. J. Neurotrauma 33 (4), 346–353. https://doi.org/10.1089/neu.2015.3880.

Kramer, J.H., Jurik, J., Sha, S.J., et al., 2003. Distinctive neuropsychological patterns in frontotemporal dementia, semantic dementia, and alzheimer disease. Cogn. Behav. Neurol. Off. J. Soc. Behav. Cogn. Neurol. 16 (4), 211–218.

La Joie, R., Ayakta, N., Seeley, W.W., et al., 2019. Multisite study of the relationships between antemortem [11C]PIB-PET centiloid values and postmortem measures of alzheimer's disease neuropathology. Alzheimers Dement. J. Alzheimers Assoc. 15 (2), 205–216. https://doi.org/10.1016/j.jalz.2018.09.001.

La Joie, R., Bejanin, A., Fagan, A.M., et al., December 2017. Associations between [18F]AV1451 tau PET and CSF measures of tau pathology in a clinical sample. Neurology. https://doi.org/10.1212/WNL.0000000000004860.

La Joie, R., Bejanin, A., Fagan, A.M., et al., 2018. Associations between [18F]AV1451 tau PET and CSF measures of tau pathology in a clinical sample. Neurology 90 (4), e282–e290. https://doi.org/10.1212/WNL.0000000000004860.

La Joie, R., Perrotin, A., Barré, L., et al., 2012. Region-specific hierarchy between atrophy, hypometabolism, and β-amyloid (Aβ) load in alzheimer's disease dementia. J. Neurosci. 32 (46), 16265–16273. https://doi.org/10.1523/JNEUROSCI.2170-12.2012.

Lee, C.M., Jacobs, H.I.L., Marquié, M., et al., 2018. 18F-Flortaucipir Binding in choroid plexus: related to race and hippocampus signal. J. Alzheimers Dis. JAD 62 (4), 1691–1702. https://doi.org/10.3233/JAD-170840.

Lehmann, M., Ghosh, P.M., Madison, C., et al., 2013. Diverging patterns of amyloid deposition and hypometabolism in clinical variants of probable alzheimer's disease. Brain J. Neurol. 136 (Pt 3), 844–858. https://doi.org/10.1093/brain/aws327.

Little, D.M., Geary, E.K., Moynihan, M., et al., 2014. Imaging chronic traumatic brain injury as a risk factor for neurodegeneration. Alzheimers Dement. J. Alzheimers Assoc. 10 (3 Suppl), S188–S195. https://doi.org/10.1016/j.jalz.2014.04.002.

Lockhart, S.N., Ayakta, N., Winer, J.R., La Joie, R., Rabinovici, G.D., Jagust, W.J, 2017. Elevated 18F-AV-1451 PET tracer uptake detected in incidental imaging findings. Neurology 88 (11), 1095–1097. https://doi.org/10.1212/WNL.0000000000003724.

Lowe, V.J., Curran, G., Fang, P., et al., 2016. An autoradiographic evaluation of AV-1451 Tau PET in dementia. Acta Neuropathol. Commun. 4, 58. https://doi.org/10.1186/s40478-016-0315-6.

Lowe V.J., Wiste H.J., Senjem M.L., et al. Widespread brain tau and its association with ageing, Braak stage and alzheimer's dementia. Brain. doi:10.1093/brain/awx320.

Maass, A., Landau, S., Baker, S.L., et al., 2017. Comparison of multiple tau-PET measures as biomarkers in aging and alzheimer's disease. Neuroimage 157 (Supplement C), 448–463. https://doi.org/10.1016/j.neuroimage.2017.05.058.

Makaretz, S.J., Quimby, M., Collins, J., et al., October 2017. Flortaucipir tau PET imaging in semantic variant primary progressive aphasia. J. Neurol. Neurosurg. Psychiatry. https://doi.org/10.1136/jnnp-2017-316409.

Malone, I.B., Leung, K.K., Clegg, S., et al., 2015. Accurate automatic estimation of total intracranial volume: a nuisance variable with less nuisance. Neuroimage 104, 366–372. https://doi.org/10.1016/j.neuroimage.2014.09.034.

Marquié, M., Normandin, M.D., Vanderburg, C.R., et al., 2015. Validating novel tau positron emission tomography tracer [F-18]-AV-1451 (T807) on postmortem brain tissue. Ann. Neurol. 78 (5), 787–800. https://doi.org/10.1002/ana.24517.

Marquié, M., Verwer, E.E., Meltzer, A.C., et al., 2017. Lessons learned about [F-18]-AV-1451 off-target binding from an autopsy-confirmed parkinson's case. Acta Neuropathol. Commun. 5 (1), 75. https://doi.org/10.1186/s40478-017-0482-0.

McKee, A.C., Stein, T.D., Nowinski, C.J., et al., 2013. The spectrum of disease in chronic traumatic encephalopathy. Brain 136 (1), 43–64. https://doi.org/10.1093/brain/aws307.

McKee, A.C., Stern, R.A., Nowinski, C.J., et al., 2013. The spectrum of disease in chronic traumatic encephalopathy. Brain J. Neurol. 136 (Pt 1), 43–64. https://doi.org/10.1093/brain/aws307.

Mckee, A.C., Abdolmohammadi, B., Stein, T.D., 2018. The neuropathology of chronic traumatic encephalopathy. Handb. Clin. Neurol. 158, 297–307. https://doi.org/10.1016/B978-0-444-63954-7.00028-8.

McKhann, G.M., Knopman, D.S., Chertkow, H., et al., 2011. The diagnosis of dementia due to alzheimer's disease: recommendations from the National Institute on Aging-Alzheimer's Association workgroups on diagnostic guidelines for alzheimer's disease. Alzheimers Dement. 7 (3), 263–269. https://doi.org/10.1016/j.jalz.2011.03.005.

Mez, J., Solomon, T.M., Daneshvar, D.H., et al., 2015. Assessing clinicopathological correlation in chronic traumatic encephalopathy: rationale and methods for the Unite study. Alzheimers Res. Ther. 7 (1), 62. https://doi.org/10.1186/s13195-015-0148-8.

Mez, J., Daneshvar, D.H., Kiernan, P.T., et al., 2017. Clinicopathological evaluation of chronic traumatic encephalopathy in players of American football. JAMA 318 (4), 360–370.

Mez, J., Daneshvar, D.H., Kiernan, P.T., et al., 2017. Clinicopathological evaluation of chronic traumatic encephalopathy in players of American football. JAMA 318 (4), 360–370. https://doi.org/10.1001/jama.2017.8334.

Mitsis, E.M., Riggio, S., Kostakoglu, L., et al., 2014. Tauopathy PET and amyloid PET in the diagnosis of chronic traumatic encephalopathies: studies of a retired NFL player and of a man with FTD and a severe head injury. Transl. Psychiatry 4, e441. https://doi.org/10.1038/tp.2014.91.

Montenigro, P.H., Baugh, C.M., Daneshvar, D.H., et al., 2014. Clinical subtypes of chronic traumatic encephalopathy: literature review and proposed research diagnostic criteria for traumatic encephalopathy syndrome. Alzheimers Res. Ther. 6 (5), 68. https://doi.org/10.1186/s13195-014-0068-z.

Morris, J.C., 1993. The clinical dementia rating (CDR): current version and scoring rules. Neurology 43 (11), 2412–2414.

Omalu, B., Small, G.W., Bailes, J., et al., November 2017. Postmortem autopsy-confirmation of antemortem [F-18]FDDNP-PET scans in a football player with chronic traumatic encephalopathy. Neurosurgery. https://doi.org/10.1093/neuros/nyx536.

Orrison, W.W., Hanson, E.H., Alamo, T., et al., 2009. Traumatic brain injury: a review and high-field MRI findings in 100 unarmed combatants using a literature-based checklist approach. J. Neurotrauma 26 (5), 689–701. https://doi.org/10.1089/neu.2008.0636.

Ossenkoppele, R., Tolboom, N., Foster-Dingley, J.C., et al., 2012. Longitudinal imaging of alzheimer pathology using [11C]PIB, [18F]FDDNP and [18F]FDG PET. Eur. J. Nucl. Med. Mol. Imaging 39 (6), 990–1000. https://doi.org/10.1007/s00259-012-2102-3.

Ossenkoppele, R., Schonhaut, D.R., Schöll, M., et al., 2016. Tau PET patterns mirror clinical and neuroanatomical variability in alzheimer's disease. Brain J. Neurol. 139 (Pt 5), 1551–1567. https://doi.org/10.1093/brain/aww027.

Ossenkoppele, R., Schonhaut, D.R., Schöll, M., et al., 2016. Tau PET patterns mirror clinical and neuroanatomical variability in alzheimer's disease. Brain J. Neurol. 139 (Pt 5), 1551–1567. https://doi.org/10.1093/brain/aww027.

Peskind, E.R., Petrie, E.C., Cross, D.J., et al., 2011. Cerebrocerebellar hypometabolism associated with repetitive blast exposure mild traumatic brain injury in 12 Iraq war Veterans with persistent post-concussive symptoms. Neuroimage 54 (Suppl 1), S76–S82. https://doi.org/10.1016/j.neuroimage.2010.04.008.

Potvin, O., Dieumegarde, L., Duchesne, S., 2017. Alzheimer's disease neuroimaging initiative. Normative morphometric data for cerebral cortical areas over the lifetime of the adult human brain. Neuroimage 156, 315–339. https://doi.org/10.1016/j.neuroimage.2017.05.019.

Provenzano, F.A., Jordan, B., Tikofsky, R.S., Saxena, C., Van Heertum, R.L., Ichise, M, 2010. F-18 FDG PET imaging of chronic traumatic brain injury in boxers: a statistical parametric analysis. Nucl. Med. Commun. 31 (11), 952–957. https://doi.org/10.1097/MNM.0b013e32833e37c4.

Rabinovici, G.D., Rosen, H.J., Alkalay, A., et al., 2011. Amyloid vs FDG-PET in the differential diagnosis of AD and FTLD. Neurology 77 (23), 2034–2042. https://doi.org/10.1212/WNL.0b013e31823b9c5e.

Rabinovici, G.D., Stephens, M.L., Possin, K.L, 2015. Executive dysfunction. Contin. Minneap. Minn. 21 (3 Behavioral Neurology and Neuropsychiatry), 646–659. https://doi.org/10.1212/01.CON.0000466658.05156.54.

Reams, N., Eckner, J.T., Almeida, A.A., et al., 2016. A clinical approach to the diagnosis of traumatic encephalopathy syndrome (TES). JAMA Neurol. 73 (6), 743–749. https://doi.org/10.1001/jamaneurol.2015.5015.

Register-Mihalik, J.K., Guskiewicz, K.M., McLeod, T.C.V., Linnan, L.A., Mueller, F.O., Marshall, S.W, 2013. Knowledge, attitude, and concussion-reporting behaviors among high school athletes: a preliminary study. J. Athl. Train. 48 (5), 645–653. https://doi.org/10.4085/1062-6050-48.3.20.

Roberts, G.W., Gentleman, S.M., Lynch, A., Graham, D.I, 1991. beta A4 amyloid protein deposition in brain after head trauma. Lancet Lond. Engl. 338 (8780), 1422–1423.

Roberts, G.W., Gentleman, S.M., Lynch, A., Murray, L., Landon, M., Graham, D.I, 1994. Beta amyloid protein deposition in the brain after severe head injury: implications for the pathogenesis of alzheimer's disease. J. Neurol. Neurosurg. Psychiatry 57 (4), 419–425.

Sander, K., Lashley, T., Gami, P., et al., 2016. Characterization of tau positron emission tomography tracer [18F]AV-1451 binding to postmortem tissue in alzheimer's disease, primary tauopathies, and other dementias. Alzheimers Dement. J. Alzheimers Assoc. 12 (11), 1116–1124. https://doi.org/10.1016/j.jalz.2016.01.003.

Schonhaut, D.R., McMillan, C.T., Spina, S., et al., 2017. 18F-flortaucipir tau positron emission tomography distinguishes established progressive supranuclear palsy from controls and parkinson disease: a multicenter study. Ann. Neurol. 82 (4), 622–634. https://doi.org/10.1002/ana.25060.

Seo, S.W., Ayakta, N., Grinberg, L.T., et al., 2017. Regional correlations between [11C] PIB PET and post-mortem burden of amyloid-beta pathology in a diverse neuropathological cohort. NeuroImage Clin. 13, 130–137. https://doi.org/10.1016/j.nicl.2016.11.008.

Small, G.W., Kepe, V., Siddarth, P., et al., 2013. PET scanning of brain tau in retired national football league players: preliminary findings. Am. J. Geriatr. Psychiatry 21 (2), 138–144. https://doi.org/10.1016/j.jagp.2012.11.019.

Smid, L.M., Vovko, T.D., Popovic, M., et al., 2006. The 2,6-disubstituted naphthalene derivative FDDNP labeling reliably predicts Congo red birefringence of protein deposits in brain sections of selected human neurodegenerative diseases. Brain Pathol. Zurich Switz. 16 (2), 124–130. https://doi.org/10.1111/j.1750-3639.2006.00006.x.

Smith, R., Schöll, M., Widner, H., et al., 2017. In vivo retention of18F-AV-1451 in corticobasal syndrome. Neurology 89 (8), 845–853. https://doi.org/10.1212/WNL.0000000000004264.

Staffaroni, A.M., Brown, J.A., Casaletto, K.B., et al., February 2018. The longitudinal trajectory of default mode network connectivity in healthy older adults varies as a function of age and is associated with changes in episodic memory and processing speed. J. Neurosci. 3067–3117. https://doi.org/10.1523/JNEUROSCI.3067-17.2018.

Stein, T.D., Montenigro, P.H., Alvarez, V.E., et al., 2015. Beta-amyloid deposition in chronic traumatic encephalopathy. Acta Neuropathol. (Berl.) 130 (1), 21–34. https://doi.org/10.1007/s00401-015-1435-y.

Stern, R.A., Adler, C.H., Chen, K., et al., 2019. Tau positron-emission tomography in former national football league players. N. Engl. J. Med. 0https://doi.org/10.1056/NEJMoa1900757. (0):null.

Stroop, J.R., 1935. Studies of interference in serial verbal reactions. J. Exp. Psychol. 18 (6), 643–662. https://doi.org/10.1037/h0054651.

The DIAGNOSE-CTE Research Project - Full Text View - ClinicalTrials.gov. https://clinicaltrials.gov/ct2/show/NCT02798185. Accessed May 21, 2018.

Utianski, R.L., Whitwell, J.L., Schwarz, C.G., et al., 2018. Tau-PET imaging with [18F]AV-1451 in primary progressive apraxia of speech. Cortex J. Devoted Study Nerv. Syst. Behav. 99, 358–374. https://doi.org/10.1016/j.cortex.2017.12.021.

Victoroff, J, 2013. Traumatic encephalopathy: review and provisional research diagnostic criteria. NeuroRehabilitation 32 (2), 211–224. https://doi.org/10.3233/NRE-130839.

Xia, M., Wang, J., He, Y, 2013. BrainNet viewer: a network visualization tool for human brain connectomics. PLoS ONE 8 (7), e68910. https://doi.org/10.1371/journal.pone.0068910.

Yesavage, J.A., Brink, T.L., Rose, T.L., et al., 1982. Development and validation of a geriatric depression screening scale: a preliminary report. J. Psychiatr. Res. 17 (1), 37–49.